Electronic structure of ReS_2 and $ReSe_2$ from first-principles calculations, photoelectron spectroscopy, and electrolyte electroreflectance

C. H. Ho* and Y. S. Huang†
Department of Electronic Engineering, National Taiwan University of Science and Technology, Taipei 106, Taiwan, Republic of China

J. L. Chen and T. E. Dann
Synchrotron Radiation Research Center, Hsinchu 300, Taiwan, Republic of China

K. K. Tiong
Department of Electrical Engineering, National Taiwan Ocean University, Keelung 202, Taiwan, Republic of China
(Received 27 May 1999)

The electronic structures of ReS_2 and $ReSe_2$ single crystals are investigated using a first-principles density-of-states (DOS) calculation, ultraviolet photoelectron spectroscopy (UPS), and electrolyte electroreflectance (EER). The total and partial DOS were calculated by the full-potential linearized-augmented-plane-wave method. From the calculations, the main contribution near the band edge of ReX_2 ($X=$S,Se) is determined to be dominated by the nonbonding Re *d* orbitals. The valence-band DOS is experimentally verified by the UPS measurements. EER measurements were performed in the energy range of 1.3–6 eV. The EER spectra exhibit sharp derivativelike structures in the vicinity of the band-edge excitonic transitions as well as higher-lying interband transitions. Transition energies are determined accurately. From the experimental and the theoretically calculated results, probable energy-band structures of ReS_2 and $ReSe_2$ are constructed.
[S0163-1829(99)07847-9]

I. INTRODUCTION

ReS_2 and $ReSe_2$ are diamagnetic indirect semiconductors belonging to the family of transition-metal dichalcogenides crystallized in a distorted layered structure of triclinic symmetry (space group $P\bar{1}$). In recent investigations, these compounds have been attractive as electrode or photoelectrode materials because of their catalytic properties and favorable stability.[1–4] Photoelectrochemical spectral response measurements showed that ReS_2 and $ReSe_2$ single crystals had an enhanced stability against photocorrosion with respect to other semiconductors such as CdS and GaAs.[5] The chemical stability is mainly attributed to the chemically saturated surface of the crystals in connection with some *d* character of the bonding. Furthermore, ReS_2 is of considerable interest as a catalytic material having potential application as a sulfur-tolerant hydrogenation and hydrodesulfurization catalyst[1,6] and as a promising solar-cell material in electrochemical cells.[4,7]

ReX_2 can be thought of as distorted $1T$-MX_2 dichalcogenides.[6] The $1T$-MX_2 phase consists of edge-shared MX_6 octahedra. In each MX_2 layer, the metal-atom sheet is sandwiched by chalcogen-atom sheets and the metal atoms of an undistorted MX_2 layer form a hexagonal lattice. ReX_2 have a d^3 electron count; the metal atoms in the metal sheet slip off their regular sites comprising a Re_4 ''diamond unit'' and resulting in a shorter Re-Re distance.[8] These Re_4 ''diamonds'' are coplanar and coupled with one another to form a one-dimensional clustering pattern of ''diamond chains.'' The diamond-chain clusters in the metal sheets of ReX_2 resulted in a lattice distortion from the perfect octahedral layered structure. The structural information on $ReSe_2$ was first determined by Alcock and Kjekshus.[9] They proposed that the distortion of $ReSe_2$ bonds was related to the movement of the rhenium atoms toward each other. Wildervanck and Jellinek[1] showed that ReS_2 and $ReSe_2$ are isostructural and crystallized in a distorted $CdCl_2$ structure of triclinic symmetry. Lamfers *et al.*[10] reported the structural data of ReX_2 using single-crystal x-ray diffraction and claimed that for ReS_2 there are two sandwiches in a unit cell related by symmetry center. However, from the recent study of the crystal structure of $ReS_{2-x}Se_x$ layered series by powder x-ray diffraction,[11] the whole series of $ReS_{2-x}Se_x$ single crystals were shown to be single phase and isostructural. The structural data of binary compounds ReS_2 and $ReSe_2$ were determined to be similar to the results of Wildervanck and Jellinek.[1]

The energy-band structure is one of the most important factors in determining the solid-state properties of a material. In this paper we evaluate the electronic structures of ReS_2 and $ReSe_2$ using the density-of-states (DOS) calculations, the ultraviolet photoelectron spectroscopy (UPS), and electrolyte-electroreflectance (EER) measurements. The total and partial density of states of the semiconducting layered compounds ReS_2 and $ReSe_2$ were numerically calculated self-consistently with the full-potential linearized-augmented-plane-wave (LAPW) method.[12] For the experimental analysis, UPS is employed to extract information on the valence-band electronic structure of the material. The electronic band structure of the material is being probed by the EER technique. The EER technique has been proven to be a very powerful tool in the study of the band structure of semiconductors.[13,14] The derivative nature of EER spectra suppresses uninteresting background effects and greatly en-

hances the precision in the determination of transition energies. The shaper line shapes as compared to the conventional optical techniques have enabled us to achieve a greater resolution and hence to detect weaker features. Subsequently, from the EER spectra of ReS_2 and $ReSe_2$ we observed more features which were not detected by the UPS measurements. The EER spectra can be fitted with a form of the Aspnes equation of the derivative Lorentzian line shape.[15] From a detailed line-shape fit, the transition energies of the band-edge excitonic and higher-lying interband transitions are determined accurately. From the experimentally and theoretically calculated results, together with the results of previous optical-absorption measurements,[16] probable band-structure schemes for ReS_2 and $ReSe_2$ are constructed.

II. EXPERIMENTAL DETAIL AND DOS CALCULATION

Single crystals of ReS_2 and $ReSe_2$ were grown using the chemical vapor transport method with Br_2 as the transport agent. Prior to crystal growth, quartz tubes containing bromine and the elements (Re: 99.95% pure, S: 99.999%, Se: 99.999%) were evacuated and sealed. To improve the stoichiometry, sulfur or selenium with 2 mol % in excess was added with respect to rhenium. The quartz tube was placed in a three-zone furnace and the charge prereacted for 24 h at 800 °C while the temperature of the growth zone was set at 1000 °C to prevent the transport of the product. The furnace was then equilibrated to give a constant temperature across the reaction tube, and was programmed over 24 h to produce the temperature gradient at which single-crystal growth takes place. The best results were obtained with temperature gradients of about $1060 \rightarrow 1010\,^{\circ}C$ for ReS_2 and $1050 \rightarrow 1000\,^{\circ}C$ for $ReSe_2$. Both ReS_2 and $ReSe_2$ formed thin, silver-colored, graphitelike, hexagonal platelets up to 2 cm^2 in area and 100 μm in thickness. X-ray-diffraction patterns of single crystals were obtained using Ni-filtered Cu $K\alpha$ radiation. The patterns confirmed the triclinic symmetry of ReS_2 and $ReSe_2$ with all parameters consistent with those previously reported.[2,9] Electron probe microanalysis indicated a chalcogen deficiency in the crystals. Hall effect measurements revealed *n*-type semiconducting behavior. Optical-absorption measurements showed indirect semiconducting behavior with an energy gap of 1.37 eV for ReS_2 and 1.19 eV for $ReSe_2$.

For the computational work, we utilized WIEN97 software to calculate the electronic band structure and density of states for ReS_2 and $ReSe_2$. This program package is capable of performing the electronic structure calculations of solids using the full-potential LAPW method.[12] Since the layered materials are characterized by strong covalent intralayer bonding and weak van der Waals interlayer interactions, the calculation of the electronic band structure for single-layer ReX_2 was employed. In this paper the electronic-structure calculations were performed using LAPW method with the structural data from Table I as the input parameters. By incorporating the information of lattice parameters, space group, and atomic coordination of ReS_2 and $ReSe_2$ into the WIEN97 software, the partial density of states of Re atoms and chalcogen atoms and total density of states of ReX_2 compounds are respectively determined.

The energy distribution of the photoelectrons will provide information on the density of states in the electronic structure of materials. In this study, the ultraviolet light source was derived from the synchrotron radiation source by the LSGM beamline at the Synchrotron Radiation Research Center (SRRC). The light source provides an ultraviolet ray in the energy range of 15–200 eV and a spot size of $\sim 1.5 \times 1.5\,mm^2$. The crystals were cleaved and placed in a highly evacuated chamber with a pressure of $\sim 8 \times 10^{-11}$ Torr. The monochromatic ultraviolet beam is filtered by a spherical grating monochromator, and a VSW hemispherical collector of a multichannel analyzer collected the emitted photoelectrons. The measurements were done on an as-grown (001) surface with the photon incidence angle kept at 20° and the detection angle at 45°. The incident photon energies for measuring the photoelectrons of the valence band and Re $4f$ core levels were fixed at 50 and 100 eV, respectively. The UPS spectra were deduced from the electron counts in various channels of the analyzer with an energy resolution of 0.05 eV.

TABLE I. Input parameters for the DOS calculations of ReX_2.

Material		ReS_2	$ReSe_2$
Lattice parameters	a (Å)	6.450	6.713
	b (Å)	6.390	6.623
	c (Å)	6.403	6.740
	α (deg)	105.49	104.59
	β (deg)	91.32	92.28
	γ (deg)	119.03	118.79
Space group		$P\bar{1}$	$P\bar{1}$

The EER spectra were taken on a fully computerized setup for modulation spectroscopy described elsewhere.[17] The detector response to the dc component of the reflected light is kept constant by either an electronic servo mechanism or a neutral density filter so that the ac reflectance corresponds to $\Delta R/R$, the differential reflectance. Scans of $\Delta R/R$ versus wavelength are obtained using a 0.35 m McPherson grating monochromator together with an Oriel 150 W xenon arc lamp as a monochromatic light source. Phase-sensitive detection is used to measure the differential reflectance. Plate-shaped crystals were selected for EER measurements. The electrolyte was a 1 N H_2SO_4 aqueous solution, and the counter electrode was a 5 cm^2 platinum (Pt) plate. A 200 Hz, 100 mV peak-to-peak square wave with $V_{dc}=0$ V versus Pt electrode was used to modulate the electric field in the space-charge region of the ReS_2 or $ReSe_2$ electrodes. The magnitude of the modulated field across the space-charge region must be maintained such that the EER line shape remains invariant and the amplitude of $\Delta R/R$ varies linearly with the modulation voltages.

III. RESULTS AND DISCUSSION

Displayed in Figs. 1(a) and 1(b) are the UPS spectra and the calculated DOS for ReS_2 and $ReSe_2$ in the energy range near the valence band. The dotted lines in Fig. 1 correspond to the DOS of the compounds ReX_2 (X=S or Se), the solid lines are those of metal Re atoms, and the dashed lines are the calculated DOS of chalcogen atoms. The experimental

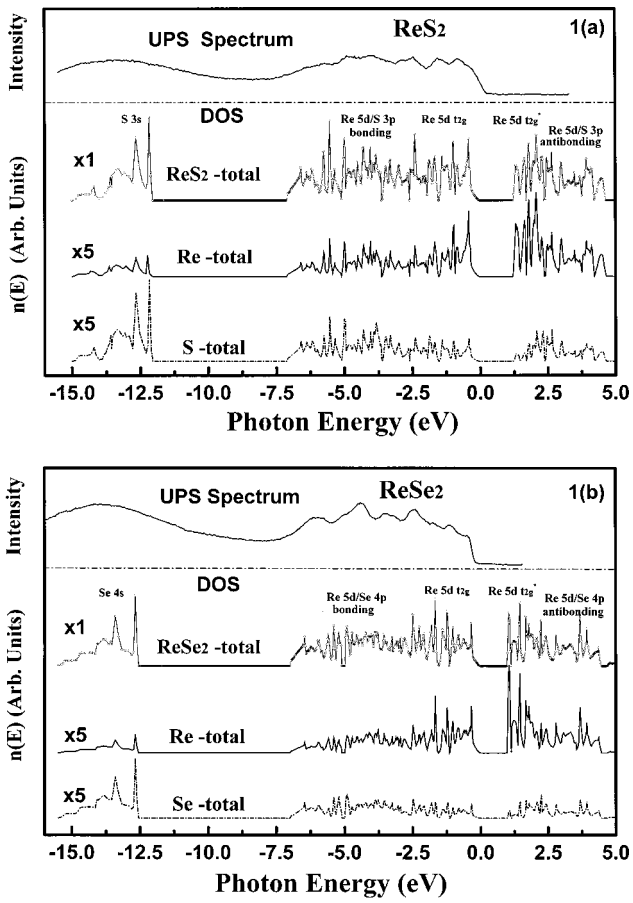

FIG. 1. The experimental UPS spectra (upper parts) and calculated density of states (lower parts) for (a) ReS_2 and (b) $ReSe_2$. The dotted lines in the lower parts correspond to the DOS of the compounds $Re\,X_2$ (X=S or Se), the solid lines are those of metal Re atoms, and the dashed lines are the calculated DOS of chalcogen atoms.

UPS spectra and the calculated DOS exhibit a multitude of sharp features which are due to the triclinic low-symmetry structures of $Re\,X_2$. Figure 1 also indicates a broad and flat region of the valence-band UPS spectra of $Re\,X_2$, which is due to the three d electrons of the rhenium atom whose effect is extended over the entire valence band and strongly hybridized with the S $3p$ (Se $4p$) states. This is a consequence of a stronger overlap of the wave functions of Re $5d$ orbitals owing to the shorter Re-Re distances. Through UPS measurements, the work functions of the materials can be determined from the minimum photoionization energies of the collected photoelectrons. The work functions for ReS_2 and $ReSe_2$ are estimated to be 5.75 and 5.6 eV, respectively. From the DOS calculation, the widths of the valence band are 7.05 eV for ReS_2 and 6.9 eV for $ReSe_2$. These results agreed well with the UPS measurements. For $Re\,X_2$, the S $3s$ (Se $4s$) band ranges from -13.2 to -16.1 eV (-13.4 to -16.3 eV) with respect to the Fermi level located at the bottom of the conduction band. The calculated results also reveal that the contributions of Re atoms (solid lines) near the top portions of the valence band and the lowest portions of the conduction band are much larger than those of chalcogen atoms (dashed lines). The other parts of the valence and conduction bands are dominated by the contributions of

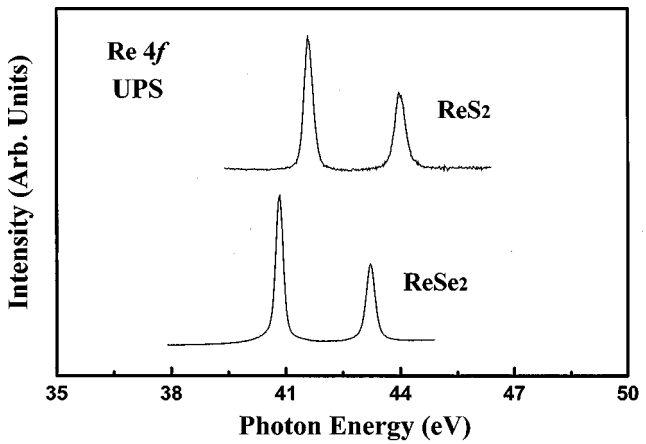

FIG. 2. Ultraviolet photoelectron spectra of the Re $4f$ core levels of ReS_2 and $ReSe_2$.

Re $5d\,e_g/X\,p$ complexes. From the DOS calculations, the energy gaps of ReS_2 and $ReSe_2$ are determined to be 1.16 and 0.89 eV, respectively. The gap energy of 0.89 eV for $ReSe_2$ is in approximate agreement with the value of 0.87 eV calculated for the same crystal by Kertesz *et al.*[8] where a simple tight-binding band-structure calculation of extended Hückel type is being employed. Recently, Raybaud *et al.*[18] reported *ab initio* density-functional studies of the electronic structure

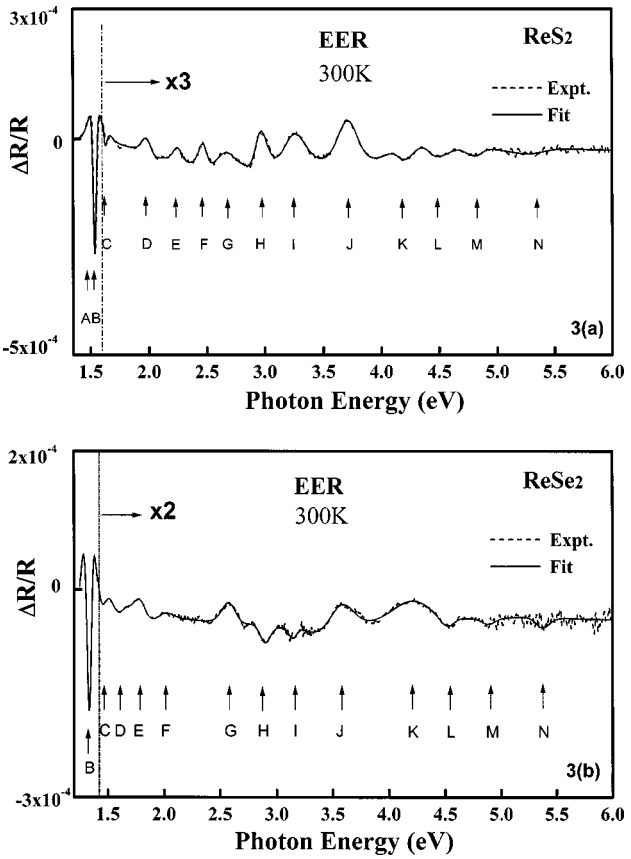

FIG. 3. The EER spectra (dashed lines) of (a) ReS_2 and (b) $ReSe_2$ at room temperature in the range of 1.3–6.0 eV. The solid lines are least-squares fits to the Aspnes derivative line-shape functional form. The obtained transition energies are indicated by arrows.

TABLE II. Energy positions of various features observed in the EER spectrum of ReS_2 and the assignments of interband transitions.

Feature	Energy (eV)	The assignments of interband transitions
A (E_1^{ex})	1.486 ± 0.005	Nonbonding Re $5d\,t_{2g}$→Nonbonding Re $5d\,t_{2g}^*$
B (E_2^{ex})	1.534 ± 0.005	Nonbonding Re $5d\,t_{2g}$→Nonbonding Re $5d\,t_{2g}^*$
C (E^{ex})	1.621 ± 0.005	Nonbonding Re $5d\,t_{2g}$→Sulfur $3p$ states
D	1.988 ± 0.01	Re $5d$/S $3p$ bonding→Re $5d$/S $3p$ antibonding
E	2.249 ± 0.01	Re $5d$/S $3p$ bonding→Re $5d$/S $3p$ antibonding
F	2.474 ± 0.01	Re $5d$/S $3p$ bonding→Re $5d$/S $3p$ antibonding
G	2.684 ± 0.01	Re $5d$/S $3p$ bonding→Re $5d$/S $3p$ antibonding
H	2.952 ± 0.01	Re $5d$/S $3p$ bonding→Re $5d$/S $3p$ antibonding
I	3.241 ± 0.01	Re $5d$/S $3p$ bonding→Re $5d$/S $3p$ antibonding
J	3.716 ± 0.01	Re $5d$/S $3p$ bonding→Re $5d$/S $3p$ antibonding
K	4.166 ± 0.01	Re $5d$/S $3p$ bonding→Re $5d$/S $3p$ antibonding
L	4.486 ± 0.01	Re $5d$/S $3p$ bonding→Re $5d$/S $3p$ antibonding
M	4.830 ± 0.01	Re $5d$/S $3p$ bonding→Re $5d$/S $3p$ antibonding
N	5.344 ± 0.015	Re $5d$/S $3p$ bonding→Re $5d$/S $3p$ antibonding

of ReS_2. The calculated energy gap of 1.16 eV agreed well with our present DOS calculation for the same material. The electronic structure of ReS_2 is found to be determined by short-range interactions in the S $3p$– Re $5d$ band complex with the ligand-field splitting of the Re $5d$ states in the environment of the S atoms determining the structure of the d band. The total and partial density of states were calculated. Furthermore, *ab initio* band-structure calculations of ReX_2 were also performed by Fang *et al.*[19] The total and partial DOS of undistorted $3R$-ReX_2 and distorted ReX_2 were, respectively, calculated by the localized-spherical-wave method.[19] From the calculations, the energy gap and the width of the valence band for the distorted ReS_2 ($ReSe_2$) were determined to be 1.0 eV (0.5 eV) and 7.05 eV (6.8 eV), respectively. The results also showed that the conduction band is composed mainly of Re $5d$ states mixed with a small amount of chalcogen p orbitals. For ReX_2, neither the top of the valence band nor the bottom of the conduction band is at the Γ point. Our results of the total and partial DOS calculations for ReS_2 and $ReSe_2$ using the LAPW are in reasonable agreement with these reports.

ReS_2 and $ReSe_2$ are found to be indirect semiconductors with an optical gap of 1.37 and 1.19 eV, respectively.[16] The formation of a semiconducting gap is due to the formation of triclinic low symmetry in the ReS_2 and $ReSe_2$ isoelectronic compounds. These triclinic structures can be considered as arising from a deformation of the octahedral stacking formula of layered dichalcogenides. The triclinic structure is derived from the octahedral layered structure by a shift of Re atoms to form Re_4 units in the central plane of the X-M-X sandwich. Because of the Re-Re interactions, the energy can be lowered by forming a gap in the middle of bonding and antibonding t_{2g} bands. The bonding t_{2g} band overlaps strongly with the $X\,p$ band and constitutes the valence band; the antibonding t_{2g} band together with the $X\,p$– Re e_g hybrid states form the conduction band. The highest occupied states around the Fermi level are d_{xy} and $d_{x^2-y^2}$ orbitals.[8,18] The contribution of chalcogen p_z orbitals is much stronger at the

TABLE III. Energy positions of various features observed in the EER spectrum of $ReSe_2$ and the assignments of interband transitions.

Feature	Energy (eV)	The assignments of interband transitions
B (E_2^{ex})	1.339 ± 0.005	Nonbonding Re $5d\,t_{2g}$→Nonbonding Re $5d\,t_{2g}^*$
C (E^{ex})	1.458 ± 0.005	Nonbonding Re $5d\,t_{2g}$→Selenium $4p$ states
D	1.616 ± 0.01	Re $5d$/Se $4p$ bonding→Re $5d$/Se $4p$ antibonding
E	1.782 ± 0.01	Re $5d$/Se $4p$ bonding→Re $5d$/Se $4p$ antibonding
F	2.002 ± 0.01	Re $5d$/Se $4p$ bonding→Re $5d$/Se $4p$ antibonding
G	2.585 ± 0.01	Re $5d$/Se $4p$ bonding→Re $5d$/Se $4p$ antibonding
H	2.891 ± 0.01	Re $5d$/Se $4p$ bonding→Re $5d$/Se $4p$ antibonding
I	3.154 ± 0.01	Re $5d$/Se $4p$ bonding→Re $5d$/Se $4p$ antibonding
J	3.561 ± 0.01	Re $5d$/Se $4p$ bonding→Re $5d$/Se $4p$ antibonding
K	4.230 ± 0.01	Re $5d$/Se $4p$ bonding→Re $5d$/Se $4p$ antibonding
L	4.544 ± 0.01	Re $5d$/Se $4p$ bonding→Re $5d$/Se $4p$ antibonding
M	4.88 ± 0.01	Re $5d$/Se $4p$ bonding→Re $5d$/Se $4p$ antibonding
N	5.365 ± 0.015	Re $5d$/Se $4p$ bonding→Re $5d$/Se $4p$ antibonding

top portion of the valence band than at the bottom portion of the conduction band. For the p_x and p_y orbitals, the top portion of the valence band has nearly equal contributions from all chalcogen atoms.

Displayed in Fig. 2 are the ultraviolet photoelectron spectra of the Re $4f$ core-level electrons for ReS_2 and $ReSe_2$. For both spectra, two peaks are observed and the peak splittings (Re $4f_{7/2}$ and $4f_{5/2}$) for ReS_2 and $ReSe_2$ have the same value of 2.4 eV. The energy positions of the two peaks for $ReSe_2$ showed a redshift of ~0.8 eV with respect to ReS_2 and are, respectively, located at 40.83 and 43.23 eV. For the Re metal, the peak positions of the $4f$ core level are 40.5 and 42.9 eV.[20] In comparison with the Re metal, the energy shifts 3/4 of the $4f$ core levels are most probably influenced by the bonding of the chalcogen elements with rhenium in the Re X_2 compounds. The linewidths of the $4f$ core levels for Re X_2 are estimated to be 0.12 eV for the lower-energy peak and 0.25 eV for the higher one. From the linewidth broadening, the energy resolutions of our UPS spectra are higher than the XPS data reported by Fang *et al.*[19]

In order to evaluate the electronic band structure, EER measurements of ReS_2 and $ReSe_2$ were also carried out. Four samples of each material from different growth batches were chosen. All four samples exhibited similar spectral responses. The typical EER spectra of ReS_2 and $ReSe_2$ at room temperature in the energy range of 1.3–6 eV are shown in Figs. 3(a) and 3(b), respectively. In comparison with the UPS results, more features are detected in the EER spectra and the derivativelike structures are apparent in the vicinity of interband transitions. The structures are indicated by arrows and with the letters $A-N$ for ReS_2 and $B-N$ for $ReSe_2$ (as shown in Fig. 3). A multitude of interband transitions are observed as a consequence of the nature of triclinic low-symmetric structures of Re X_2. The amplitudes of two features (A and B) below 1.55 eV for ReS_2 and one feature (B) below 1.45 eV for $ReSe_2$ are much larger than other features. These features are related to the previously identified band-edge excitonic transitions E_1^{ex} and E_2^{ex}.[21] For $ReSe_2$, only E_2^{ex} is visible at 300 K, whereas for ReS_2 both E_1^{ex} and E_2^{ex} need to be included for a good fit of the features. By fitting the EER spectra with the Aspnes derivative line-shape expressions,[15] we can determine the position of the interband transitions to an accuracy better than 5 meV. Listed in Tables II and III are, respectively, the energy positions of interband transitions for ReS_2 and $ReSe_2$ obtained from the EER spectra together with the assignments of the origin of the interband transitions. Comparing the results with those of the calculated DOS of ReS_2 and $ReSe_2$, it is possible to associate the features of the EER spectra with appropriate interband transitions. At present, the results may not indicate the exact location of the critical point transitions associated with each feature. Nevertheless, this work will prove to be useful in aiding such identification when a more detailed theoretical band-structure calculation is available. We can relate the most prominent features A at 1.486 eV and B at 1.534 eV in Fig. 3(a), and the feature B at 1.339 eV in Fig. 3(b) as the band-edge excitons originated from the nonbonding Re $5d\,t_{2g}(d_{xy},d_{x^2-y^2})$ to $5d\,t_{2g}^*$ transitions. It is noticed that the feature C in Figs. 3(a) and 3(b) is being assigned as the Re d to X p interband excitonic transition. The reason for

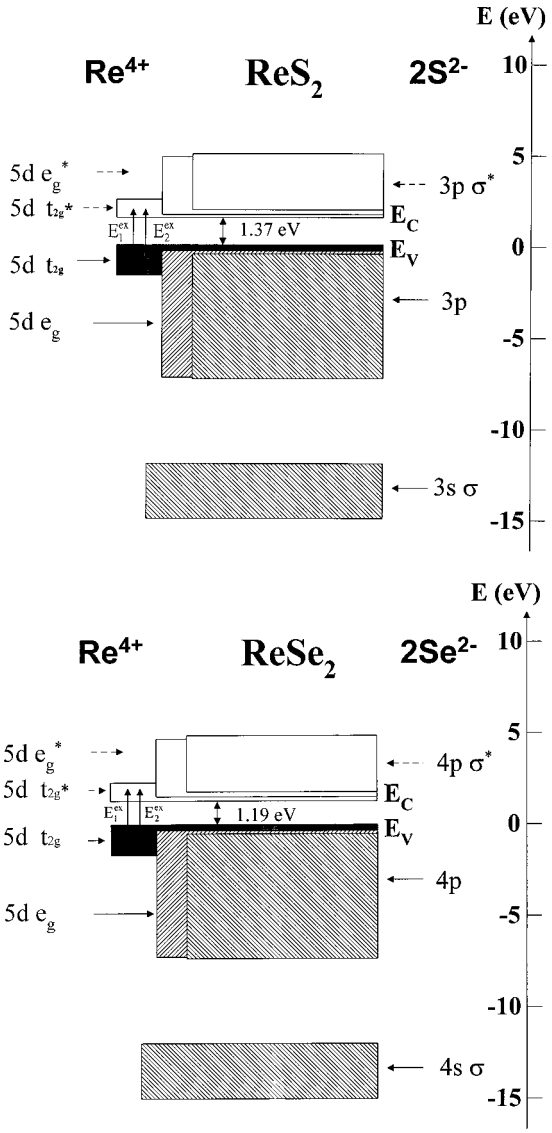

FIG. 4. The energy-band-structure schemes of (a) ReS_2 and (b) $ReSe_2$.

such an assignment is suggested by the low-temperature piezoreflectance (P_2R) measurements where a series of sharp features are observed at the energy location above E_2^{ex}.[22] From the EER spectra in Fig. 3, the structures at higher energies (i.e., features $D-N$ for ReS_2 and $ReSe_2$) are attributed to interband transitions from states of largely chalcogen X p character to (Re $5d\,e_g^*$)–($X\,p$) hybrid states. With the results of DOS calculations, EER measurements, and the optical-absorption measurements, probable band-structure schemes consistent with Table II for ReS_2 and Table III for $ReSe_2$ are constructed and are shown in Figs. 4(a) and 4(b), respectively. The band structures of ReS_2 and $ReSe_2$ are composed of three main bands separated by energy gaps. The lowest band consists of two S $3s$ or Se $4s$ bands; the next bands are mainly S $3p$ or Se $4p$ hybridized with Re $5d$. Three Re $5d$ orbitals form a nonbonding t_{2g} band with d_{z^2} at the bottom hybridized with S $3p$ or Se $4p$ and $d_{x^2-y^2}$ and d_{xy} at the top of the band. The bottom of the conduction band is composed mainly of Re $5d$ states mixed with a small amount of S $3p$ or Se $4p$ orbitals. Energy gaps of 1.37 and 1.19 eV

separated the top of the valence band and the bottom of the conduction band for ReS_2 and $ReSe_2$, respectively. The antibonding Re $5d\ t_{2g}^*$ band overlaps with the Re $5d\ e_g^*$ band.

IV. SUMMARY

In summary, the experimental UPS and EER measurements and theoretical calculation of DOS of ReS_2 and $ReSe_2$ have been carried out. A multitude of structures in the UPS spectra and calculated DOS are observed due to the triclinic low-symmetry structures of these materials. The contributions in the top portions of the valence band and the lowest portions of the conduction band mainly come from the nonbonding Re $5d$ orbitals. From the results of EER and previous optical-absorption measurements with appropriate transition assignments, probable energy-band-structure schemes for ReS_2 and $ReSe_2$, respectively, are constructed.

ACKNOWLEDGMENTS

The authors C.H.H. and Y.S.H. acknowledge the support of the National Science Council of the Republic of China under Project No. NSC88-2112-M-011-001 and K.K.T. acknowledges the support of the National Science Council of the Republic of China under Project No. NSC88-2112-M-019-004.

*Present address: Department of Electronic Engineering, Kuang Wu Institute of Technology and Commerce, Peitou, Taipei 112, Taiwan, Republic of China.

†Author to whom correspondence should be addressed. Electronic address: ysh@et.ntust.edu.tw

[1] J. C. Wildervanck and F. Jellinek, J. Less-Common Met. **24**, 73 (1971).

[2] S. P. Kelty, A. F. Ruppert, R. R. Chianelli, J. Ren, and M.-H. Whangboo, J. Am. Chem. Soc. **116**, 7857 (1994).

[3] J. V. Marzik, R. Kershaw, K. Dwight, and A. Wold, J. Solid State Chem. **51**, 170 (1984).

[4] H. S. Broadbent, L. H. Slangh, and N. L. Jarvis, J. Am. Chem. Soc. **76**, 1519 (1954).

[5] S. Harris and R. R. Chianelli, J. Catal. **86**, 400 (1984).

[6] B. L. Wheeler, J. K. Leand, and A. J. Bard, J. Electrochem. Soc. **133**, 358 (1986).

[7] F. P. Koffyberg, K. Dwight, and A. Wold, Solid State Commun. **30**, 433 (1979).

[8] M. Kertesz and R. Hoffmann, J. Am. Chem. Soc. **106**, 3453 (1984).

[9] N. W. Alcock and A. Kjekshus, Acta Chem. Scand. **19**, 79 (1965).

[10] H.-J. Lamfers, A. Meetsma, G. A. Wiegers, and J. L. de Boer, J. Alloys Compd. **241**, 34 (1996).

[11] C. H. Ho, Y. S. Huang, P. C. Liao, and K. K. Tiong, J. Phys. Chem. Solids **60**, 1797 (1999).

[12] P. Blaha, K. Schwarz, and J. Luitz, WIEN97—A Full-Potential Linearized Augmented Plane Wave Package for Calculating Crystal Properties, Vienna University of Technology, Vienna, Austria (1997).

[13] M. Cardona, K. L. Shaklee, and F. H. Pollak, Phys. Rev. **154**, 696 (1967).

[14] Y. S. Huang and Y. F. Chen, Phys. Rev. B **38**, 7997 (1988).

[15] D. E. Aspnes, in *Handbook on Semiconductors*, edited by M. Balkanski (North-Holland, Amsterdam, 1980), Vol. 2, p. 109.

[16] C. H. Ho, P. C. Liao, Y. S. Huang, T. R. Yang, and K. K. Tiong, J. Appl. Phys. **81**, 6380 (1997).

[17] Y. S. Huang, H. M. Chen, C. J. Chang, and G. J. Jan, Chin. J. Phys. **23**, 144 (1985).

[18] P. Raybaud, J. Hafner, G. Kresse, and H. Troulhoat, J. Phys.: Condens. Matter **9**, 11 107 (1997).

[19] C. M. Fang, G. A. Wiegers, C. Haas, and R. A. de Groot, J. Phys.: Condens. Matter **9**, 4411 (1997).

[20] C. D. Wagner, W. M. Riggs, L. E. Davis, J. F. Moulder, and G. E. Muilenberg, *Handbook of X-ray Photoelectron Spectroscopy* (Perkin-Elmer, Eden Prairie, MN, 1978).

[21] C. H. Ho, P. C. Liao, Y. S. Huang, and K. K. Tiong, Phys. Rev. B **55**, 15 608 (1997).

[22] C. H. Ho, Y. S. Huang, K. K. Tiong, and P. C. Liao, J. Phys.: Condens. Matter **11**, 5367 (1999).